A Comparison of Three Classes of Spectrum Sensing Techniques

Takeshi Ikuma and Mort Naraghi-Pour

Department of Electrical and Computer Engineering
Louisiana State University
Baton Rouge, LA 70803
Email: {tikuma@lsu.edu, mort@ece.lsu.edu}

***Abstract*—Spectrum sensing is used to identify the (temporarily) unused (licensed) frequency bands and as such plays a key role in dynamic spectrum access. Spectrum sensing is currently being investigated by a number of researchers. In this paper we compare the performance of three classes of algorithms—energy detectors, autocorrelation detectors, and the cyclic autocorrelation detector. The focus of the study is on the trade-offs of the three approaches under fixed false alarm and detection probabilities.**

***Index Terms*—Spectrum Sensing, Dynamic Spectrum Access, Cognitive Radio**

I. Introduction

Cognitive radios are envisioned to provide opportunistic spectrum access by extending the underutilized, licensed frequency bands to unlicensed (secondary) users. To this end, a key component of the cognitive radio technology is a spectrum sensing technique used by the secondary user to detect the unused frequency bands (the so called white spaces).

There are four basic types of non-cooperative spectrum sensing techniques: energy detector, autocorrelation detector, cyclostationary feature detector, and matched-filter detector. The energy detector [1], [2] is one of the simplest techniques to detect the presence of a signal if the noise power at the receiver is known. However, uncertainty in the noise power can significantly degrade the performance of energy detectors. While the noise power can be estimated, the estimation error may lead to the so called signal-to-noise ratio (SNR) wall [3]. The matched-filter detector requires the full extent of the parameters of the primary user's signal, which is not generally available to the cognitive radio. Since this requirement limits the applicability of of matched detectors, they have not been included in this study.

The cyclostationary feature detector relies on the cyclostationary nature of communication signals. In particular, the Dandawaté-Giannakis method utilizes the cyclic autocorrelation function of the received signal at one cycle frequency [4]. We note that recently extensions to this algorithm have been presented which take advantage of multiple cycle frequencies in order to improve the performance of the detector [5], [6]. More recently, an autocorrelation detector was introduced in [7], [8]. This approach relies on the fact that the autocorrelation function of the oversampled communication signal exhibits non-zero values at non-zero lags, whereas for the white noise (i.e., no signal) these values will be zero. While the computational complexity of the autocorrelation-based method is comparable to that of the energy detector, it does not require knowledge of the noise power.

In this paper, our goal is to compare the performance of three spectrum sensing techniques, namely the energy detector, the cyclic autocorrelation detector [4], and the autocorrelation detector [8]. In particular, we compare the required SNR for each technique in order to achieve a given probability of false alarm P_{fa} and a probability of detection P_d. Also, spectrum agility of cognitive radios demands a fast and efficient spectrum sensing technique; the latter depends on the number of signal samples that must be collected for the detection algorithm. We, therefore, compare the number of signal samples required by each of the three methods in order to achieve a given probability of false alarm P_{fa} and the probability of detection P_d.

The remainder of this paper is organized as follows. Section II describes the spectrum sensing problem, and Section III introduces the algorithms under consideration. These algorithms are compared in Section IV, followed by concluding remarks in Section VII.

II. Spectrum Sensing Problem

For the purpose of spectrum sensing, the RF front-end of the receiver can be simplified as shown as in Fig. 1. The radio receives an RF signal $r(t)$, which may contain a primary communication signal with center frequency f_c Hz and bandwidth $(-f_b, f_b)$ Hz. After down conversion, (ideal) low-pass filtering, and sampling, the radio obtains the complex baseband signal $\{x_n\}$. The bandwidth of the low-pass filter is $(-f_{bw}, f_{bw})$ Hz, and the sampling period is given by $T_s \triangleq (2f_{bw})^{-1}$.

The spectrum sensing algorithm processes the complex baseband signal x_n, given by

$$x_n = \eta s_n + v_n \tag{1}$$

where s_n is the primary baseband communication signal and v_n is the complex noise process. The value of $\eta \in \{0, 1\}$ determines the presence or absence of the primary signal s_n.

978-1-4244-2324-8/08/$25.00 © 2008 IEEE.

This full text paper was peer reviewed at the direction of IEEE Communications Society subject matter experts for publication in the IEEE "GLOBECOM" 2008 proceedings.

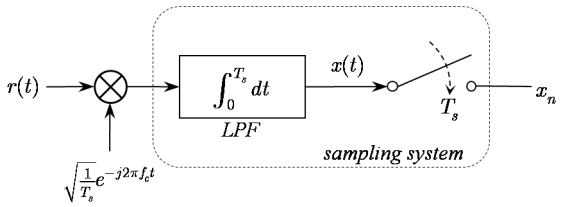

Fig. 1. Simplified block diagram of ideal RF front-end.

Therefore, the detection of the primary signal is described by the following binary hypotheses testing problem.

$$\begin{array}{ll} H_0: & \eta = 0, \quad \text{primary signal absent} \\ H_1: & \eta = 1, \quad \text{primary signal present} \end{array} \tag{2}$$

The primary signal $\{s_n\}$ is unknown and is modeled as a complex-valued zero-mean wide-sense stationary (WSS) process, characterized by its autocorrelation function $r_{ss,l} \triangleq E[s_n s^*_{n-l}]$. Furthermore, $\{s_n\}$ is band-limited in the frequency range $(-\omega_b, \omega_b)$ rad/sample where $\omega_b \triangleq \pi f_b / f_{bw}$, and $0 < \omega_b < \pi$. The band-limited nature of s_n guarantees that s_n is non-white, i.e., $r_{ss,l} \neq \sigma_s^2 \delta_l$ where σ_s^2 is the signal power and δ_l is the Kronecker delta function.

Alternatively, $\{s_n\}$ can also be modeled as a cyclostationary process (instead of a WSS process) [9]. Then, $\{s_n\}$ is characterized by its cyclic-autocorrelation function

$$r_{xx,l}(\alpha) \triangleq \lim_{T\to\infty} \frac{1}{T} \sum_{n=0}^{T} E[x_n x^*_{n-l}] e^{-j\alpha n} \tag{3}$$

where α is a cyclic frequency.

The complex-valued noise process $\{v_n\}$ is modeled as an i.i.d. circular white Gaussian noise process with mean zero and variance σ_v^2. Therefore, the autocorrelation function of the noise process is given by $r_{nn,l} = \sigma_v^2 \delta_l$, and the cyclic-autocorrelation function of $\{v_n\}$ is given by $r_{nn,l}(\alpha) = \sigma_v^2 \delta_l \delta(\alpha)$ where $\delta(\alpha)$ denotes the Dirac delta function.

Assuming that $\{s_n\}$ and $\{v_n\}$ are uncorrelated, we express the conditional autocorrelation function of x_n as

$$r_{xx,l|H_\eta} = \eta r_{ss,l} + \sigma_v^2 \delta_l \tag{4}$$

and the conditional cyclic-autocorrelation function of x_n as

$$r_{xx,l|H_\eta}(\alpha) = \eta r_{ss,l}(\alpha) + \sigma_v^2 \delta_l \delta(\alpha). \tag{5}$$

The SNR of x_n is denoted by

$$\gamma \triangleq \frac{\sigma_s^2}{\sigma_v^2}. \tag{6}$$

One of our goals in this paper is to study the effect of the signal bandwidth ω_b (in rad/sample) on the performance of the sensing algorithm. Consequently, we will utilize the ratio of signal energy to noise power spectral density (PSD), E_s/N_0, which is related to γ by

$$\frac{E_s}{N_0} = \gamma \frac{\pi}{\omega_b}. \tag{7}$$

In other words, assuming constant E_s/N_0, the SNR is proportional to the ratio of the sampling rate and signal bandwidth and is maximized when the sampling rate matches the signal bandwidth (i.e., $\omega_b = \pi$).

Taking N samples of x_n, $\mathbf{x} = (x_0, x_1, \cdots, x_{N-1})$, a spectrum sensing algorithm forms a decision statistic $T(\mathbf{x})$ and compares it to a threshold λ, i.e.,

$$\begin{array}{ll} T(\mathbf{x}) \; \begin{array}{l} < \lambda \\ \geq \lambda \end{array} & \begin{array}{l} \text{decide } H_0 \\ \text{decide } H_1. \end{array} \end{array} \tag{8}$$

For ease of notation, in the following we will drop the dependence of the decision statistic on the sample data $\mathbf{x}$. The performance of spectrum sensing algorithm is determined by the probabilities of false alarm and detection given by

$$P_{fa}(\lambda) \triangleq Pr\{T > \lambda | H_0\} \tag{9}$$

and

$$P_d(\lambda) \triangleq Pr\{T > \lambda | H_1\}. \tag{10}$$

III. Spectrum Sensing Algorithms

This section summarizes the three spectrum sensing algorithms under study. The description includes formulation of the decision statistics and (asymptotic) analytical expressions for probabilities of false alarm and detection.

A. Energy Detector

Urkowitz [1] analyzed the energy detection method in the continuous-time domain; in this paper, however, we follow the discrete-time baseband model of Digham et al. [2]. With a noise power estimate $\hat{\sigma}_v^2$, the decision statistic is given by

$$T_{ED} \triangleq \frac{2}{\hat{\sigma}_v^2} \sum_{n=0}^{N-1} |x_n|^2. \tag{11}$$

The performance of this detector is obtained in [2] assuming that the noise power is perfectly known (i.e., $\hat{\sigma}_v^2 = \sigma_v^2$). Under H_0, this decision statistic is chi-square distributed with $2N$ degrees of freedom while under H_1 it is non-central chi-square distributed with $2N$ degrees of freedom and $2N\gamma$ as the non-centrality parameter. We note that the gain term $2/\sigma_v^2$ in (11) is introduced so that the decision statistics are drawn from standard chi-square distributions. Consequently, the probability of false alarm given a threshold λ_{ED} is determined as

$$P_{fa,ED}(\lambda_{ED}) = 1 - P\left(\frac{\lambda_{ED}}{2}, N\right) \tag{12}$$

where $P(a, x)$ is the (lower) incomplete gamma function [10, §6.5.1]. Likewise, the probability of detection given a threshold λ_{ED} is determined as

$$P_{d,ED}(\lambda_{ED}) = Q_N\left(\sqrt{2N\gamma}, \sqrt{\lambda_{ED}}\right) \tag{13}$$

where $Q_m(\alpha, \beta)$ is the generalized Marcum Q-function [11, p.12].

The challenge in utilizing this simple and efficient detector is the uncertainty in the noise power [3]. Since the exact noise level is unknown to the detector, the noise power must be

This full text paper was peer reviewed at the direction of IEEE Communications Society subject matter experts for publication in the IEEE "GLOBECOM" 2008 proceedings.

estimated. The estimation error causes the so-called "SNR wall" [3] in the detection performance. The term "SNR wall" refers to the fact that the target pair of detection and false-alarm probabilities become unattainable below a certain SNR bound regardless of how many samples are accumulated.

We consider the Tandra-Sahai worst-case performance of the energy detector [3]. In their model, the actual noise power σ_v^2 is bounded in the interval $[(1/\rho)\sigma_v^2, \rho\sigma_v^2]$ where $\rho > 1$ quantifies the noise uncertainty. Accordingly, the worst-case false-alarm occurs when $\hat{\sigma}_v^2 = \rho\sigma_v^2$ while the worst-case detection occurs when $\hat{\sigma}_v^2 = (1/\rho)\sigma_v^2$. This leads to the worst-case probabilities of false alarm and of detection:[1]

$$P_{fa,ED}^{(\text{w.c.})}(\lambda_{ED}, \rho) = 1 - P\left(\frac{\lambda_{ED}}{2\rho}, N\right), \tag{14}$$

and

$$P_{d,ED}^{(\text{w.c.})}(\lambda_{ED}, \rho) = Q_N\left(\sqrt{2N\gamma}, \sqrt{\lambda_{ED}\rho}.\right) \tag{15}$$

These worst-case probabilities will be used to illustrate the impact of uncertainty in noise power on the performance of energy detectors with respect to the performance of the noise-power independent detectors.

B. Autocorrelation Detector

Using the samples in $\mathbf{x}$, the autocorrelation function at some lag l can be estimated from

$$\hat{r}_l(\mathbf{x}) \triangleq \begin{cases} \frac{1}{N-l}\sum_{n=0}^{N-l-1} x_{n+l}x_n^*, & l \geqslant 0 \\ \hat{r}_{-l}^*, & l < 0 \end{cases} \tag{16}$$

We note that $\hat{r}_l$ is an unbiased and consistent estimator of $r_{xx,l}$. Under the null hypothesis, $\hat{r}_l = 0$ for all $l \neq 0$. On the other hand, assuming that $\{s_n\}$ is non-white, under the alternate hypothesis, $\hat{r}_l \neq 0$ for some $l \neq 0$. By further assuming that the primary baseband signal $\{s_n\}$ is lowpass and complex-valued with independent real and imaginary components, we can show that $r_{xx,l|H_\eta}$ is real-valued [8]. Therefore, we form the following autocorrelation-based decision statistic[2]

$$T_{AC} \triangleq \sum_{l=1}^{L} w_l \frac{\text{Re}\{\hat{r}_l\}}{\hat{r}_0} \tag{17}$$

Scaling by $\hat{r}_0$ ensures that the algorithm is a constant false-alarm rate (CFAR) detector. The parameter L should be chosen so that $r_{l|H_1} > 0$ for all $l \leq L$. While the weighting coefficients w_l could be computed to achieve the optimal performance, we have opted to use

$$w_l \triangleq \frac{L + 1 - |l|}{L + 1}. \tag{18}$$

With decision threshold λ_{AC}, the probability of false alarm of this detector is

$$P_{fa,AC}(\lambda_{AC}) = Q\left(\lambda_{AC}\left[\frac{\lambda_{AC}^2}{N} + \frac{1}{2N}\sum_{i=1}^{L} w_i^2\right]^{-\frac{1}{2}}\right) \tag{19}$$

[1]We should point out that (14) and (15) are exact expressions, whereas in [3], invoking the central limit theorem,the probabilities are obtained assuming Gaussian distributions.

[2]T_{AC} is a special case of $T_{IN}(\omega)$ in [8], viz, setting $\omega = 0$ of [8, (17)].

The probability of detection, on the other hand, is found as

$$P_{d,AC}(\lambda_{AC}) = Q\left(\frac{-\mathbf{w}^T(\lambda_{AC})\bar{\mathbf{z}}_1}{\sqrt{\mathbf{w}^T(\lambda_{AC})\mathbf{C}_1\mathbf{w}(\lambda_{AC})}}\right) \tag{20}$$

where ^{T} denotes transpose,

$$\mathbf{w}(\lambda) = \begin{bmatrix}-\lambda & w_1 & \cdots & w_L\end{bmatrix}^T, \tag{21}$$

$$\bar{\mathbf{z}}_1 = \begin{bmatrix}1 & 0 & \cdots & 0\end{bmatrix}^T + \gamma\begin{bmatrix}1 & \rho_{r,1} & \cdots \rho_{r,L}\end{bmatrix}^T, \tag{22}$$

and

$$\mathbf{C}_1 = \frac{1}{2N}\,\text{diag}(\begin{bmatrix}2 & 1 & \cdots & 1\end{bmatrix}^T) + \frac{\gamma}{N}[\mathcal{T}\{\mathbf{p}_{0,L}, \mathbf{p}_{0,L}^T\} + \mathcal{H}\{\mathbf{p}_{0,L}, \mathbf{p}_{L,2L}^T\}] \tag{23}$$

with $\rho_{r,l} = \text{Re}\{r_{s,l}\}/\sigma_s^2$ and

$$\mathbf{p}_{a,b} \triangleq \begin{bmatrix}\rho_{r,a} & \rho_{r,a+1} & \cdots & \rho_{r,b}\end{bmatrix}]^T \tag{24}$$

In (23), $\text{diag}(\mathbf{d})$ forms a diagonal matrix with d_i as (i,i)-th element of the matrix, $\mathcal{T}(\mathbf{c}, \mathbf{r})$ represents a Toeplitz matrix with the first column $\mathbf{c}$ and the first row $\mathbf{r}$, and $\mathcal{H}(\mathbf{c}, \mathbf{r})$ represents a Hankel matrix with the first column $\mathbf{c}$ and the last row $\mathbf{r}$.

C. Cyclic Autocorrelation Detector

The cyclic autocorrelation function $r_{xx,l}(\alpha)$ of x_n at some lag l and some cyclic frequency α can be estimated from samples $\mathbf{x}$ by

$$\hat{r}_l(\alpha) \triangleq \begin{cases} \frac{1}{N-l}\sum_{n=0}^{N-l-1} x_{n+l}x_n^* e^{-j\alpha n} & l \geqslant 0 \\ \hat{r}_{-l}^*(\alpha), & l < 0 \end{cases} \tag{25}$$

This estimator is unbiased and is consistent in the mean-square sense. Furthermore, by the central limit theorem, the distribution of both real and imaginary components of $\hat{r}_l(\alpha)$ tend to the Gaussian distribution as $N \to \infty$. [4]

Assuming that $\{s_n\}$ is cyclic with cycle frequency α, under H_1, there exists lag l such that $r_{xx,l}(\alpha) \neq 0$. Conversely, $r_{xx,l}(\alpha) = 0$ for all $l \neq 0$ under H_0. Hence, the detection statistic is derived from $\hat{r}_{l_k}(\alpha)$ for $k = 1, 2, ..., K$, as follows. First, the real and imaginary parts of $\hat{r}_{l_k}(\alpha)$ are separated to form the vector

$$\hat{\mathbf{r}} \triangleq \begin{bmatrix} \text{Re}\{\hat{r}_{l_1}(\alpha)\} & \text{Re}\{\hat{r}_{l_2}(\alpha)\} & \cdots & \text{Re}\{\hat{r}_{l_K}(\alpha)\} \\ \text{Im}\{\hat{r}_{l_1}(\alpha)\} & \text{Im}\{\hat{r}_{l_2}(\alpha)\} & \cdots & \text{Im}\{\hat{r}_{l_K}(\alpha)\} \end{bmatrix}^T \tag{26}$$

The decision statistic is then constructed as follows.

$$T_{DG} \triangleq \hat{\mathbf{r}}^T\hat{\mathbf{K}}^{-1}\hat{\mathbf{r}} \tag{27}$$

where

$$\hat{\mathbf{K}} \triangleq \frac{1}{2}\begin{bmatrix}\text{Re}\{\mathbf{P}+\mathbf{Q}\} & \text{Im}\{\mathbf{Q}-\mathbf{P}\} \\ \text{Im}\{\mathbf{P}+\mathbf{Q}\} & \text{Re}\{\mathbf{P}-\mathbf{Q}\}\end{bmatrix} \tag{28}$$

is an estimate of the covariance matrix $\mathbf{K} \triangleq \text{cov}\{\hat{\mathbf{r}}\}$. Here, the (p,q)-th element of $\mathbf{P}$ and $\mathbf{Q}$ are computed as follows.

$$P_{p,q} \triangleq \sum_{m=-M}^{M} f(m)\hat{r}_{l_p}(\alpha + \frac{2\pi m}{N})\hat{r}_{l_q}^*(\alpha + \frac{2\pi m}{N}) \tag{29}$$

This full text paper was peer reviewed at the direction of IEEE Communications Society subject matter experts for publication in the IEEE "GLOBECOM" 2008 proceedings.

and

$$Q_{p,q} \triangleq \sum_{m=-M}^{M} f(m)\hat{r}_{l_p}(\alpha + \frac{2\pi m}{N})\hat{r}_{l_q}(\alpha - \frac{2\pi m}{N}) \quad (30)$$

where $f(m)$ is a $(2M+1)$-element weighting function such that $\sum_{m=-M}^{M} f(m) = 1$. The weighted averaging in (29) and (30) are necessary to make the covariance estimate $\hat{\mathbf{K}}$ consistent [4].

Under H_0, the decision statistic in (27) is asymptotically chi-square distributed with $2K$ degrees of freedom as $N \to \infty$. Hence, the (asymptotic) probability of false alarm for this detector with threshold λ_{DG} is given by

$$P_{fa,DG}(\lambda_{DG}) = 1 - P\left(\frac{\lambda_{DG}}{2}, K\right) \quad (31)$$

The asymptotic decision statistic under H_1 is non-central chi-squared[3] with $2K$ degrees of freedom and with the non-centrality parameter $\mathbf{r}^T\mathbf{K}^{-1}\mathbf{r}$, where $\mathbf{r}$ is the cyclic correlation vector, i.e., $\mathbf{r} = E\{\hat{\mathbf{r}}\}$. Hence, the probability of detection for a given λ_{DG} is given by

$$P_{d,DG}(\lambda_{DG}) = Q_K\left(\sqrt{\mathbf{r}^T\mathbf{K}^{-1}\mathbf{r}}, \sqrt{\lambda_{DG}}\right) \quad (32)$$

Comparing to the other methods, the cyclic autocorrelation detector is noticeably more numerically demanding. Not only $\hat{\mathbf{K}}$ needs to be computed, but also the algorithm must compute $\hat{\mathbf{K}}^{-1}$. Also, convergence of $\hat{\mathbf{K}}$ to $\mathbf{K}$ is slow. Consequently, the actual $P_{d,DG}$ of the cyclostationary algorithm can be noticeably worse than that predicted in (32) for a small N.

IV. Numerical Results and Performance Comparisons

In this section, we evaluate the performance of the three algorithms for fixed false alarm and detection probabilities. Specifically, we choose $P_{fa} = 10^{-3}$ and $P_d = 1 - 10^{-3}$. Other parameters are evaluated by solving the P_{fa} and P_d expressions simultaneously. For those without a closed-form solution, we evaluate the parameters numerically.

The modulation scheme used by the primary user is assumed to be Quadrature phase shift keying (QPSK). Moreover, rectangular full-response pulse-shaping is assumed which results in the following autocorrelation function for $\{s_n\}$.

$$r_{ss,l} = \begin{cases} \sigma_s^2 \frac{\sin \omega_b l}{\omega_b l} & \text{if } \omega_b l \neq 0 \\ \sigma_s^2 & \text{o.w.} \end{cases} \quad (33)$$

Here, ω_b is set so that π/ω_b corresponds to the number of samples per QPSK symbol. The fundamental cycle frequency of s_n is $2\omega_b$, and we assume that this information is known a priori for the Dandawaté-Giannakis cyclic detector. Although (32) requires $\mathbf{r}$ and $\mathbf{K}$, the exact expression for $\mathbf{K}$ is not readily available. Instead, $\mathbf{r}$ and $\mathbf{K}$ are estimated via Monte-Carlo simulation, in which $\hat{\mathbf{r}}$ is collected over $10,000$ trials.

[3]This asymptotic probability distribution definition is derived directly from the asymptotic Gaussian nature of $\hat{\mathbf{r}}$ and differs from that of Dandawaté and Giannakis. In [4], they approximated the distribution under H_1 to be Gaussian with mean $\mathbf{r}^T\mathbf{K}^{-1}\mathbf{r}$ and variance $4\mathbf{r}^T\mathbf{K}^{-1}\mathbf{r}$. These mean and variance result from Gaussian approximation of the non-central chi-square distribution assuming $\mathbf{r}^T\mathbf{K}^{-1}\mathbf{r} \gg K$.

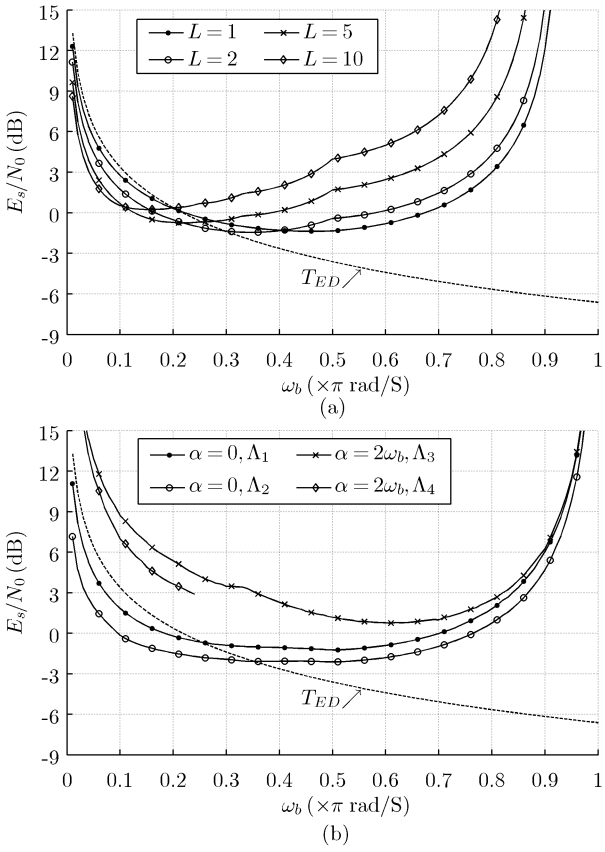

Fig. 2. E_s/N_0 vs. ω_b to maintain $P_{fa} = 10^{-3}$ and $P_d = 1 - 10^{-3}$ with $N = 1,000$: (a) autocorrelation detector T_{AC} and (b) cyclic detector T_{DG} (dotted line in both plots – T_{ED} with $\hat{\sigma}_v^2 = \sigma_v^2$).

Fig. 2 shows E_s/N_0 (required to achieve the desired P_{fa} and P_d) as a function of ω_b while $N = 1,000$ is used for all three algorithms. The dotted line in Figs. 2a and 2b shows the performance of the "ideal" energy detector, which uses the exact noise power, i.e., $\hat{\sigma}_v^2 = \sigma_v^2$. The observed dependence of the energy-detector performance on ω_b becomes apparent by substituting (7) into (13). The performance of the energy detector is optimized when $f_{bw} = f_b$ or when $\omega_b = \pi$. In this case, the required SNR is minimum given by $E_s/N_0 = -6.6$ dB. On the other hand, the performance of the energy detector deteriorates as $\omega_b \to 0$, requiring large SNR E_s/N_0 to achieve the desired performance.

Fig. 2a illustrates the performance of the autocorrelation method for $L = 1$, $L = 2$, $L = 5$, and $L = 10$. For $\omega_b > 0.3$, all configurations perform worse (significantly as $\omega_b \to 1$) than the "ideal" energy detector. The cause of the performance degradation is that as $\omega_b \to 1$, the values of the autocorrelation function $r_{xx,l}$ tend to zero for non-zero lags ($l \neq 0$). The optimal ω_b for each configuration occurs between π/L and $\pi/(L+1)$, over which $r_{xx,l} > 0$ for all $l \in \{1 : L\}$. Similar to the energy detector, for smaller ω_b, the performance deteriorates due to the excess bandwidth. The

This full text paper was peer reviewed at the direction of IEEE Communications Society subject matter experts for publication in the IEEE "GLOBECOM" 2008 proceedings.

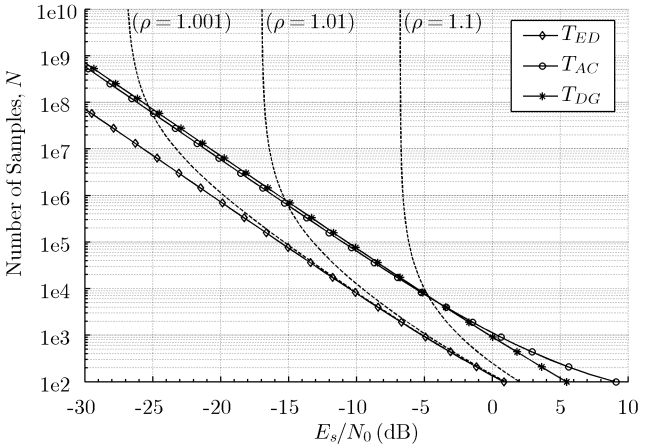

Fig. 3. E_s/N_0 vs. N under $P_{fa} = 10^{-3}$ and $P_d = 1 - 10^{-3}$: energy detector T_{ED} with $\omega_b = 1$ and $\hat{\sigma}_v^2 = \sigma_v^2$, autocorrelation detector T_{AC} with $\omega_b = \pi/3$ and $L = 2$, and cyclic detector T_{DG} with $\omega_b = \pi/3$, $\alpha = 0$, and $l_k \in \{1, 2\}$ (dotted lines – worst case T_{ED} with various ρ).

optimal performance is obtained with $L = 2$ and $\omega_b = \pi/3$.

Fig. 2b illustrates the performance of the cyclic autocorrelation detector with four configurations. The first two are configured to use $\alpha = 0$ (which means the algorithm is working on the conventional autocorrelation function) with different lag sets ($\Lambda_1 = \{1\}$ and $\Lambda_2 = \{1, 2, \ldots, 10\}$). The last two use $\alpha = 2\omega_b$, the fundamental cycle frequency, with $\Lambda_3 = \{l_0\}$ and $\Lambda_4 = \{(l_0 - 1), l_0, (l_0 + 1)\}$ where $l_0 \triangleq \text{round}\{\pi/(2\alpha)\}$. The overall behavior is similar to that of the autocorrelation detector; the detector works well over the moderate values of ω_b but suffers at both extreme values of ω_b. The algorithm detecting $\alpha = 2\omega_b$ needs significantly higher E_s/N_0 than detecting $\alpha = 0$ because $r_{ss,l}(\alpha), \alpha \neq 0$ is much smaller than $r_{ss,l}$ even at the fundamental cycle frequency. For both values of α, utilizing more correlation samples results in a lower required E_s/N_0, although the difference is not significant. We note that the last case with Λ_4 is invalid for $\omega_b > 0.25\pi$ because $\hat{\mathbf{r}}$ includes the zero-lag correlation value which is real and hence $\mathbf{K}$ becomes singular.

Next, Fig. 3 illustrates the number of samples required to achieve the desired P_{fa} and P_d for a given E_s/N_0. The parameters for the autocorrelation detector are chosen to be the optimal values found in Fig. 2a. The parameters for the cyclic autocorrelation detector, on the other hand, are selected so that the algorithm complexity (in terms of the number of samples processed) is compatible to that of the autocorrelation detector. The figure also illustrates the worst-case performance deterioration of the energy detector due to noise level uncertainty.

The "ideal" energy detector clearly outperforms (i.e., requires less number of samples) than the other two detectors if the exact value of the noise power is known. The uncertainty in the noise power estimate, as modeled by the value of ρ is also shown for the three cases of $\rho = 1.1, 1.01$, and 1.001. The autocorrelation and cyclic autocorrelation detectors with comparable configurations perform similarly but require an order of magnitude more samples to match the performance of the "ideal" energy detector. For high E_s/N_0 values, the cyclic autocorrelation detector requires fewer samples than the autocorrelation detector; however, the actual performance of the cyclic autocorrelation detector is likely to be worse as the estimate $\hat{\mathbf{K}}$ in (27) becomes less accurate with smaller N.

V. Conclusion

In this paper, we have compared the performance of three different types of spectrum sensing algorithms: the energy detector, autocorrelation detector, and the cyclic autocorrelation detector. Energy detector is by far the simplest algorithm. The detector easily outperforms the other two detectors if the noise power is perfectly known and if the signal is sampled at the rate of one sample per modulation symbol. However, in the presence of noise power uncertainty the performance of this algorithm degrades significantly. The autocorrelation detector is a true CFAR detector which does not require exact knowledge of the noise power. Furthermore, the computational complexity of this algorithm, while higher than that of the energy detector, is reasonably low. Lastly, the cyclic autocorrelation detector has an added computational complexity over the autocorrelation detector. Furthermore, the actual performance of this detector is likely to be worse than the analytical results presented here due to the on-the-fly estimation of the covariance matrix. We also found that the decision statistics at non-zero cycle frequency are much weaker than that at $\alpha = 0$, making multi-cycle alternatives less appealing.

References

[1] H. Urkowitz, "Energy detection of unknown deterministic signals," *Proceedings of the IEEE*, vol. 55, no. 4, pp. 523–531, 1967.

[2] F. F. Digham, M. S. Alouini, and M. K. Simon, "On the energy detection of unknown signals over fading channels," *IEEE Transactions on Communications*, vol. 55, no. 1, pp. 21–24, 2007.

[3] R. Tandra and A. Sahai, "SNR walls for signal detection," *IEEE J. Sel. Topics Signal Process.*, vol. 2, no. 1, pp. 4–17, 2008.

[4] A. V. Dandawaté and G. B. Giannakis, "Statistical tests for presence of cyclostationarity," *IEEE Trans. Signal Process.*, vol. 42, no. 9, pp. 2355–2369, 1994.

[5] M. Ghozzi, M. Dohler, F. Marx, and J. Palicot, "Cognitive radio: methods for the detection of free bands," *Comptes Rendus Physique*, vol. 7, no. 7, pp. 794–804, 2006.

[6] J. Lundén, V. Koivunen, A. Huttunen, and H. V. Poor, "Spectrum sensing in cognitive radios based on multiple cyclic frequencies," in *CrownCom 2007*, Orlando, FL, 2007.

[7] Y. Zeng and Y.-C. Liang, "Covariance based signal detections for cognitive radio," in *IEEE DySPAN*, Dublin, Ireland, 2007, pp. 202–207.

[8] T. Ikuma and M. Naraghi-Pour, "Autocorrelation-based spectrum sensing algorithms for cognitive radios," in *ICCCN 2008*, Submitted.

[9] W. A. Gardner, A. Napolitano, and L. Paura, "Cyclostationarity: half a century of research," *Signal Process.*, vol. 86, no. 4, pp. 639–697, 2006.

[10] M. Abramowitz and I. A. Stegun, *Handbook of Mathematical Functions with Formulas, Graphs, and Mathematical Tables*, 10th ed. Washington, D. C.: U.S. National Bureau of Standards, 1972.

[11] M. K. Simon, *Probability Distributions Involving Gaussian Random Variables*. New York: Springer Science, 2006.